Analysis by a 3D DIC technique of volumetric deformation gradients: Application to polypropylene/EPR/talc composites

Olivier de Almeida, Fabienne Lagattu, Jean Brillaud

Analysis by a 3D DIC technique of volumetric deformation gradients: Application to polypropylene/EPR/talc composites

Olivier De Almeida, Fabienne Lagattu *, Jean Brillaud

Laboratoire de Me´canique et Ingenieries, UBP et IFMA, Clermont-Ferrand, France

Abstract

A new optical device has been developed in order to measure in-plane strain fields on front and lateral faces of rectangular cross-section specimens during tension tests. It is based on digital image correlation (DIC) technique, by using a mirror reflecting the lateral grainy pattern of the specimen. Local ''true'' stress and ''true'' volumetric strain have been calculated excluding classical incompressibility or isotropy assumption. The spatial resolution reached with this technique has allowed to identify high deformation gradients in transverse directions. Front and lateral in-plane measurement fields have been projected in respective perpendicular direction, allowing the analysis of the volumetric behaviour of the studied composites for any node of a three-dimensional mesh. Applied to impact-modified polypropylene composites, this 3D DIC technique has revealed the influence of talc content on volumetric dilatation gradients.

Keywords: A. Polymer–matrix composites (PMCs); B. Plastic deformation; B. Anisotropy; Digital image correlation

1. Introduction

The heterogeneous and dilatational deformations observed in polymers, such as void growth in filled polymers and necking or crazes in homopolymers, have always encouraged the development of new techniques able to measure ''true'' strains.

From the first attempts of tracking the surface of tension specimens, assuming incompressibility and isotropic deformations [1–3], the increasing quality of digital camera allows nowadays to measure strain fields without incompressibility and/or any isotropic assumptions [4].

Many measurements have been proceeded in two dimensions on the front side of a specimen, but even if digital image correlation (DIC) has improved the spatial resolution, transverse isotropy assumption is still needed to calculate volumetric strain [5–7]. Therefore, heterogeneous microstructure induced by moulding processes is supposed not to influence plate thickness behaviour.

Based on 2D strain measurements, the 7-dots tracking technique developed by G'Sell et al. [8] has allowed for a degree of inhomogeneous axial deformation, while measuring average lateral deformation. Despite a poor spatial resolution, the in-line acquisition and calculation of this technique allows the testing machine control at constant strain rates, which is essential for modelling and numerical simulations.

Tracking pair of ink marks on two sides of rectangular bar-type specimens, Gloaguen and Lefebvre initiated the volumetric strain measurements assuming total anisotropy. However, homogeneous deformation was assumed between the two ink marks [9].

Parsons et al. have only recently obtained strain fields on both front and lateral sides of a rubber-toughened polycarbonate with one digital camera [4]. By reflecting the lateral side of the specimen with a prism perpendicular to the front surface of the specimen, they used digital image correlation to calculate volumetric strain and local transverse strains without using isotropic assumption. With a spatial

* Corresponding author. Tel.: +33 (0)5 49 49 82 39; fax: +33 (0)5 49 49 82 38.

E-mail address: fabienne.lagattu@lmpm.ensma.fr (F. Lagattu).

Table 1
Characteristics of investigated composites

Composite	Elastomer volumetric content (%)	Average diameter of elastomeric particles (μm)	Talc volumetric content (%)	Average diameter of talc plates (μm)
A	24	0.5	4	10
B	24	0.5	1	3–4

resolution of $1.4 \times 1.4\ mm^2$ on $19.05 \times 7.62 \times 3.2\ mm^3$ specimens, they concluded that transversal deformation is homogeneous in specimen's thickness.

In this study, an optical device has been developed in order to analyse deformation mechanisms of impact-modified polypropylene plates loaded in tension. These filled composites are known to present large volumetric deformation due to void formation [10–12].

Similarly to Parsons et al. [13], full-field strain measurement have been performed on both front and lateral sides of the specimen by using digital image correlation from a unique camera. Thus, no isotropic assumption is necessary to calculate volumetric dilatation. Measurements have been performed on $10 \times 10 \times 3\ mm^3$ specimens, with a spatial resolution of $0.45 \times 0.45\ mm^2$. Results show high anisotropy and high transversal deformation gradients, which have a large influence on these composite volumetric behaviours.

2. Materials and sample preparation

Materials investigated in this study are two commercial impact-modified polypropylenes used for automotive applications as car-bumpers. These composite materials supplied by Sabic are made of talc and ethylene–propylene elastomeric particles embedded in an isotactic polypropylene matrix (Table 1). The main difference between the two studied materials is that composite A contains 4% of talc, whereas composite B contains only 1%.

Both polymers were injection moulded into $300 \times 100 \times 3\ mm^3$ plates at the LRMP[1]. Tensile specimens with gauge volume dimensions $10 \times 10 \times 3\ mm^3$ were machined from the molded plates.

3. Experimental testing procedure

3.1. Experimental conditions

In order to determine full-field displacements on both front and lateral sides of the specimen, the tensile specimens have been previously covered with a random speckle pattern realised by spraying white and black powders on both sides of the specimens. It led to a white and black random grain field with an average grain diameter of 30 ± 5 μm [14].

All uniaxial tension tests have been performed on an Instron 4505 screw machine at room temperature with a constant speed of $10\ mm\ s^{-1}$. A mechanical device mounted on the testing machine supports a digital camera in front of a constant centered volume during the tension test. With this device, about 10 cm separate the CCD matrix of $2272 \times 1704\ pixels^2$ from the specimen. In this configuration, an area of $18 \times 24\ mm^2$ is in shot of the digital camera and one pattern grain is defined by about 3×3 pixels on the CCD matrix.

This set-up configuration allows to measure in-plane strains within a maximum depth of field of about 1 mm. The linear relationship between the out-of-plane movement and the parasitic induced strain indicates that out-of-plane displacements up to 1 mm only induce an in-plane strain error of about 1% [15]. Thus, in this case, the influence of out-of-plane displacements on the in-plane measurements can be neglected.

A mirror bounded up with the device has been positioned to reflect the lateral pattern of the specimen to the CCD camera (Fig. 1). The short distance between the camera and the specimen led to two different focus positions to get contrasted images of front and lateral patterns of the specimen. To bypass that difficulty, the focus distance of the camera has been adjusted using a micrometer translator without changing camera lens parameters. The scale of the "lateral pattern image" is then slightly greater than the "front pattern image" one.

Two images have been recorded at each step of the discontinuous tension tests. The influence of stress relaxation due to the tensile crosshead stops has been measured on a loaded specimen. Results have shown that if stress relaxation leads to displacement variation, it is lower than the measurement sensitivity.

3.2. Displacement field measurements

Digital image correlation consists on the measure of displacement vectors by matching subwindows of pixel

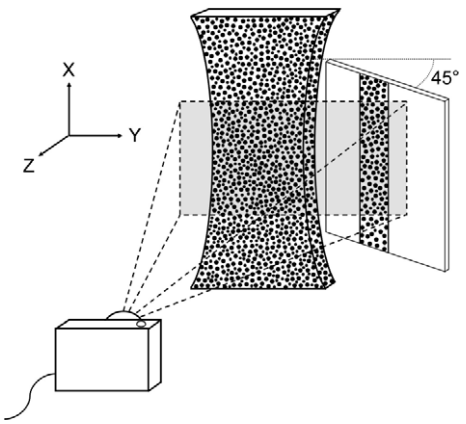

Fig. 1. Schematic representation of the experimental set-up.

[1] LRMP: Laboratoire de Rhéologie des Matières Plastiques, CNRS, UMR 5156, 23, rue du Docteur Paul Michelon, 42023 St Etienne Cedex 02, France. Tel.: +33 477481554; fax: +33 477485126.

grey-value patterns on a surface from one image to another. The displacement of each subwindow is ascribed to the centre point of the subwindow and the spatial resolution is defined as the real size of the subwindows.

The home developed software Granu is based on the direct correlation of the discrete matrix of the pixel grey levels of a subwindow. For any point $G_k\,(x_k, y_k)$ on the first picture, Granu software measures the horizontal and vertical displacements of this subwindow centre, by calculating the correlation value C_{G_k} with the subwindow centred in P_i on the second picture. The calculated correlation value is the normalized pixel-by-pixel multiplication of the two subwindows M given by

$$C_{G_k}(P_i) = \frac{C_c(M(G_k), M(P_i))}{\sqrt{C_s(M(G_k))\sqrt{C_s(M(P_i))}} \quad (1)$$

where C_c and C_s are, respectively, the cross-correlation and self-correlation functions. These functions are defined by Eqs. (2) and (3), where I represents the pixel intensity level and (u_{P_i}, v_{P_i}) are the components of the displacement vector from G_k to P_i

$$C_c(M(G_k), (M(P_i))) = \sum_{i=-\frac{N}{2}}^{\frac{N}{2}} \sum_{i=-\frac{N}{2}}^{\frac{N}{2}} I_M(x_k + i, y_k + j) \times I_M(x_k + i + u_{P_i},\ y_k + j + v_{P_i}) \quad (2)$$

$$C_s(M(G_k)) = \sum_{i=-\frac{N}{2}}^{\frac{N}{2}} \sum_{i=-\frac{N}{2}}^{\frac{N}{2}} I_M(x_k + i,\ y_k + j) \cdot I_M(x_k + i,\ y_k + j) \quad (3)$$

The Granu software is able to calculate numerous positions P_i until getting a position satisfying a threshold criterion. A systematic calculation of correlation values in a region of 7×7 pixels^2 is executed in order to distinguish erratic points. When a position P_i is pointed out to be accurate, the displacement is finally calculated at the correlation peak crest by a biparabolic fitting of this 7×7 pixels^2 correlation value surface [14].

Thereby, displacement fields can be obtained for entire mesh nodes by adjusting the threshold, depending on the image contrast and quality, and the subwindow square length N.

For all experiments, the in-plane displacement field is incrementally obtained, starting with the undeformed image, by correlating subwindows of the speckle pattern from one image to the next with an adaptive mesh. The chosen configuration used in this study allows in-plane displacement measurements with good accuracy, on both front and lateral sides of the specimens. With a magnification of 11.5 μm/pixel for front images and 11.1 μm/pixel for lateral images, the local displacements have been measured with, respectively, a spatial resolution, i.e., a correlation subwindow area, of 460×460 and 440×440 μm^2.

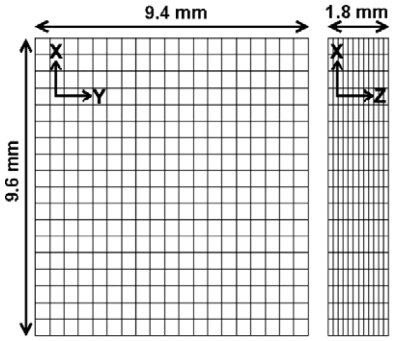

Fig. 2. Characteristics of the mesh measurement points.

Digital image correlation has been performed in about 400 measurement points on the front side and about 250 on the lateral side on areas corresponding, respectively, to 9.4×9.6 mm^2 (width × length) and 1.8×9.6 mm^2 (thickness × length) (Fig. 2). The Granu software processing time is about 5 s for 400 measurement points with a current personal computer.

In order to combine horizontal strain measurements, the scale factor between both front and lateral images has been taken into account when creating meshes. Both front and lateral meshes thus represent a same length field and any mesh line on front pattern corresponds to a line on lateral pattern.

3.3. Strain calculations

The Abaqus software is used to derive experimental data using large-strain formalisms. The Granu software has been developed in a way to treat horizontal and vertical displacements as Abaqus input file. In the Abaqus file, the subwindow centre points are written as nodes of a mesh and displacements are treated as boundary conditions.

Local true axial strains ε_{xx} are calculated on both front and lateral vertical correlations (x-axis), while local front transverse strains ε_{yy} (y-axis) and local lateral transverse strains ε_{zz} (z-axis) are, respectively, determined from horizontal front and lateral correlations.

3.4. Measurement reliability

Fig. 3 presents the local axial strains values measured in 400 points from the front pattern correlation of composite B for three different strain levels. One can see that ε_{xx} strain values dispersion increases with loading, which is in agreement with the results of Brillaud and Lagattu [14]. It leads to a relative error of about 8.8% for $\varepsilon_{xx} = 4\%$ and 5.7% for $\varepsilon_{xx} = 21\%$. This good strain resolution allows us to use an average ε_{xx} strain value.

In Fig. 4, the average axial strains measured on both front and lateral surfaces along x-axis of composite B specimen are presented for three loading levels. The good agreement of the axial strains measured from correlations on both sides validates the experimental procedure.

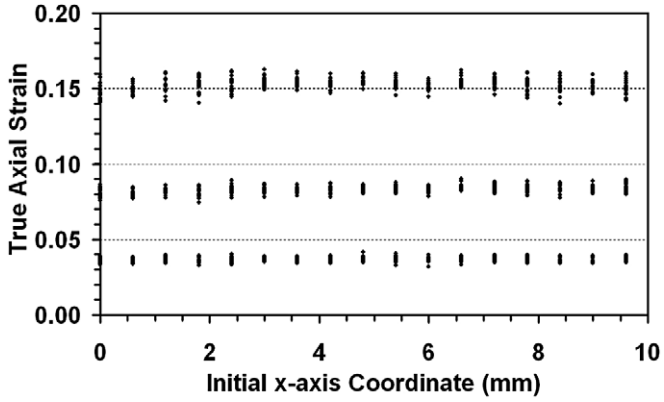

Fig. 3. Dispersion of true axial strain ε_{xx} values measured in 400 points on front side of material B for three different loading levels.

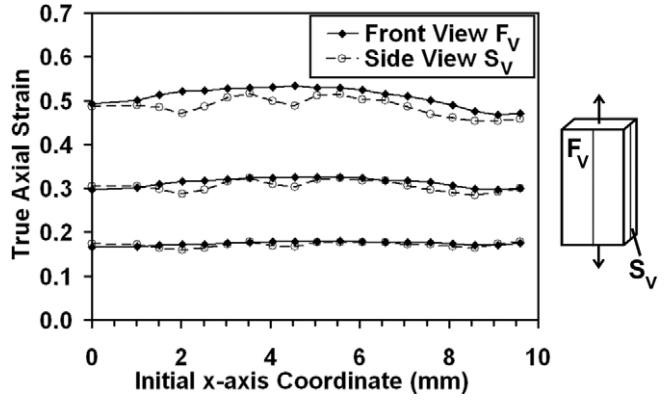

Fig. 4. True axial strain ε_{xx} measured from front and lateral pattern correlations for three loading levels in composite B.

In order to check measurement reproducibility, the same tests have been performed on three identical specimens. Fig. 5 shows the induced dispersion on transverse strain values measured for composite B. One can see that the experimental procedure leads to reproducible measured values. However, the dispersion is larger in z-axis direction for high strain level due to measurements performed on 1.8 mm of the 3 mm specimen thickness and to large transverse strain gradients.

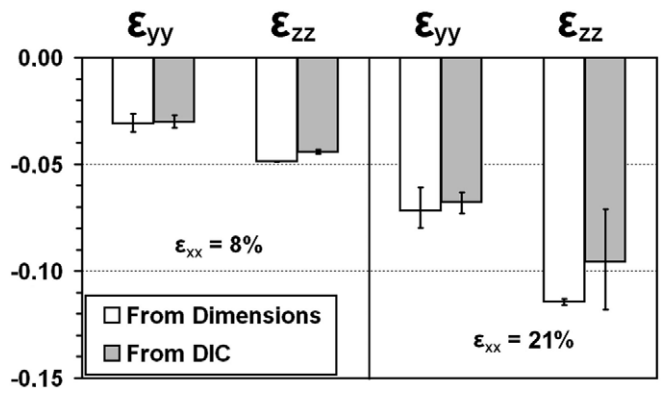

Fig. 5. Comparison for three specimens of composite B of the average transverse strains measured by DIC and of transverse strains obtained from measurements of specimen dimensions on the recorded images for two axial strain levels.

Fig. 5 also compares the DIC measurements values with global strain values obtained by measuring the specimen dimensions (width and thickness) on the recorded images. The good accordance between average DIC values and dimensions values demonstrates the method reliability.

4. Global behaviour of impact-modified polypropylenes

A first global approach has consisted in assuming a homogeneous behaviour. The average field strains have been calculated from local strains in the three directions x, y and z, afterwards called "average strains".

4.1. Anisotropic strain behaviour

Fig. 6 presents, for composites A and B, the average strains ε_{yy} and ε_{zz} as functions of average axial strain ε_{xx}. For both composites, ε_{yy} decreases continuously during tension test, while the lateral transverse strain ε_{zz} begins decreasing before stabilising. Below 10% of axial strain, both composites present a similar transverse behaviour. The deformation occurs preferentially in z-axis direction, i.e., within specimen thickness. Beyond an axial strain of 25% for composite A and 45% for composite B, the ε_{zz} stabilisation leads to a deformation process favouring specimen width reduction. These results show that the filler content influences the transverse strain behaviour of these materials: higher talc content leads to smaller strain threshold for ε_{zz} stabilisation.

4.2. True stress calculation

By using the average strains ε_{yy} and ε_{zz} measured values, the true stress σ_{xx} has been determined by calculating the cross-section area at each displacement stop. The true stress is calculated with Eq. (4), using average nominal strains ε_{yy}^{N} and ε_{zz}^{N}, and load level F reached at tension stops [12]. In Eq. (4), S_0 is the initial cross-section surface, S is

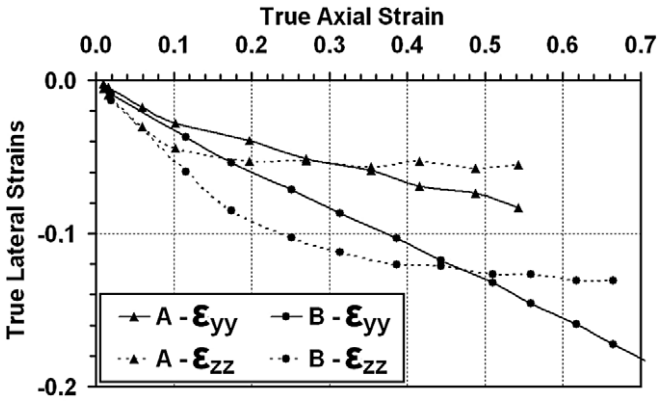

Fig. 6. Experimental average true lateral strains vs. true axial strain.

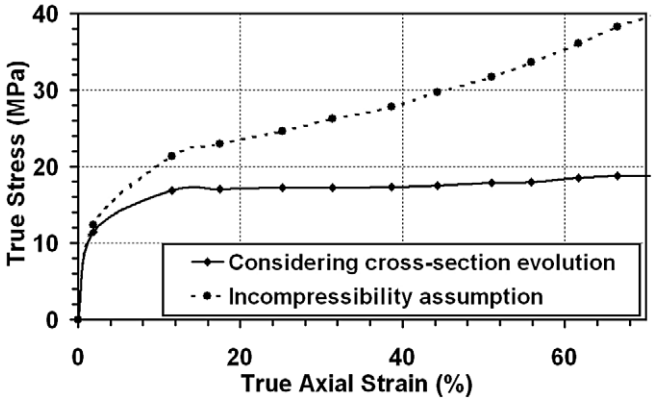

Fig. 7. Influence of incompressibility assumption on experimental stress–strain curve for composite B.

the current cross-section during tension test and W and T are, respectively, the width and the thickness of the specimens

$$\sigma_{xx} = \frac{F}{S} = \frac{F}{W \times T} = \frac{F}{S_0} \times \frac{1}{(1+\varepsilon_{yy}^{N})(1+\varepsilon_{zz}^{N})} \quad (4)$$

Fig. 7 presents the stress–strain behaviour of composite B and the influence of incompressibility on the stress level. Considering a constant Poisson's ratio of 0.5 to assume incompressibility, the stress is of course largely overestimated. Thus, compressibility needs to be considered to analyse the mechanical behaviour of these materials.

4.3. Transversal deformation gradients

The accuracy of displacement measurements allows us to analyse local strains for each width W or thickness T node lines. Fig. 8 presents true local strains ε_{yy} and ε_{zz} as front and lateral strain maps (Fig. 8a and b) and strain profiles on centered lines W and T (Fig. 8c and d). These results have been obtained for composite B loaded to 49% of average axial strain.

The anisotropic behaviour previously described also turns out to be transversally heterogeneous. Large-strain behaviour is characterized by high transverse strain gradients on both faces of the specimen. Transverse strain levels increase approaching specimen edges and the difference between maximum and minimum strains is especially marked in z-axis direction.

On front strain field (Fig. 8a and c), transverse strain ε_{yy} is mainly constant within 6 mm of field width, whereas on lateral field (Fig. 8b and d) thickness deformation behaviour is barely heterogeneous. These deformation gradients appear almost symmetrically in relation to thickness middle line. At profile T centre, the minimum strain is about zero.

Such gradients discredit classical homogeneity assumptions when strains are not measured for the entire specimen surfaces. Thus, large errors can be made calculating true stress and volumetric deformation.

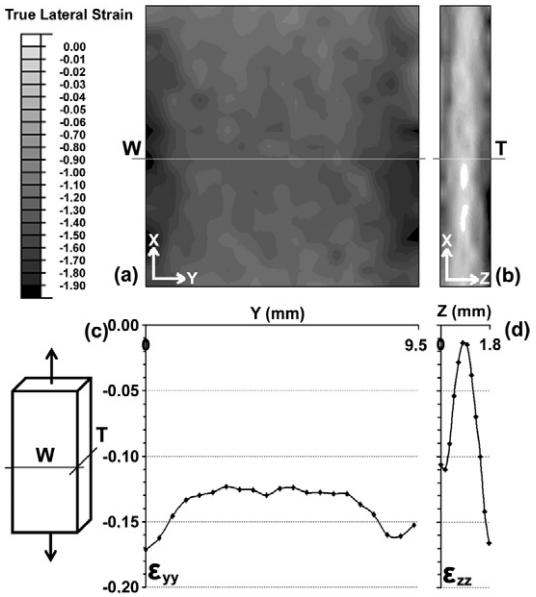

Fig. 8. Local transverse strains measured in impact-modified polypropylene B for $\varepsilon_{xx} = 49\%$ ((a) front transverse strain field ε_{yy}; (b) lateral transverse strain field ε_{zz}; (c) local front transverse strains on line W; (d) local lateral transverse strains on line T).

5. Volumetric deformation gradients in impact-modified polypropylene

5.1. Heterogeneous volumetric deformation in cross-section

Because of the large transverse strain gradients, a local volumetric approach has been preferred to analyse volumetric behaviour of impact-modified polypropylenes.

As presented in Fig. 9, the local strains measured on front and lateral correlation meshes (a) have been projected, respectively, on z- and y-axis, and the specimen can be represented as a fictive volume of $9.4 \times 9.6 \times 1.8\ \text{mm}^3$ (b) within local volumetric dilatation can be calculated for each three-dimensional mesh node (c).

Projecting the experimental front and lateral displacement fields implies that the strain fields of the specimen surfaces are assumed to be representative of the specimen core behaviour. But the inside strains are not actually measured and possible inside strain gradients cannot be ignored. Nevertheless, observations for both composites of the deformed specimen cross-sections at different strain levels by scanning electron microscopy show that the specimen cross-section remains rectangular. Thus, it allows us to neglect such possible gradients and the proposed schematic construction of the specimen volume is assumed to be representative.

The local volumetric dilatation values have been calculated by using Eq. (5), within axial and front transverse strains ε_{xx}^{N} and ε_{yy}^{N} are determined from front pattern correlation while ε_{zz}^{N} is given by lateral pattern correlation

$$\frac{\Delta V}{V_0} = (1+\varepsilon_{xx}^{N})(1+\varepsilon_{yy}^{N})(1+\varepsilon_{zz}^{N}) - 1 \quad (5)$$

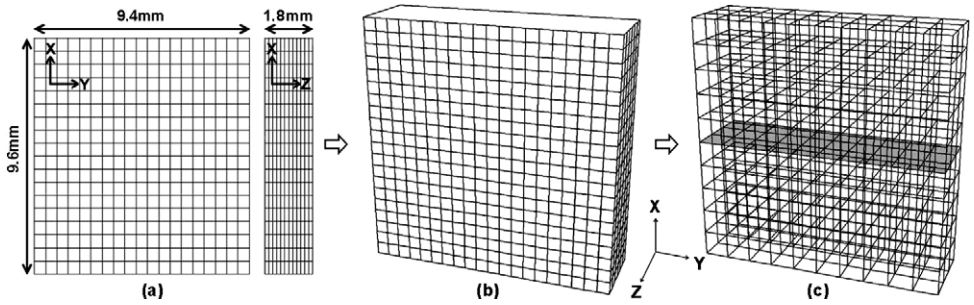

Fig. 9. Schematic representation of the experimental data extrapolation to reconstruct the specimen volume.

The experimental volumetric dilatation values in the central cross-section of the specimen are plotted in Figs. 10 and 11 for composites A and B at different loading levels.

One can see in Figs. 10 and 11 that volumetric dilatation show high gradients in these materials. These gradients increase with the average axial strain value.

For composite B, filled with only 1% of talc, the large transverse strain gradients observed on both surfaces lead to a volumetric dilatation mainly concentrated along a thickness middle line. Near specimen edges, transverse strains compensate part of axial strain, softening local volumetric dilatation. For an average axial strain of 49%, the specimen centre shows a volumetric dilatation of about 43%, whereas the specimen edges show a volumetric dilatation of about 14%.

The local volumetric dilatation gradients in composite A, which contains 4% of talc, are lower than in composite B. The thickness middle line still presents a higher volumetric dilatation level but volumetric dilatation is roughly constant in the entire specimen cross-section. For an average axial strain of 47%, the volumetric dilatation values vary from 46% to 38% from the specimen centre to the edges.

Thus, by calculating average values of volumetric dilatation, composite B exhibits a lower void formation process than composite A. That has been confirmed by measuring density on deformed samples of the two materials.

Therefore, volumetric behaviour appears to be highly influenced by filler content. Even if components of both composites are identical, the high accuracy of volumetric strain measurements has revealed two different deformation mechanisms depending on talc content.

5.2. Comparison with deformed microstructure

Fig. 12 presents the experimental values of volumetric dilatation obtained along a transverse line L in the central

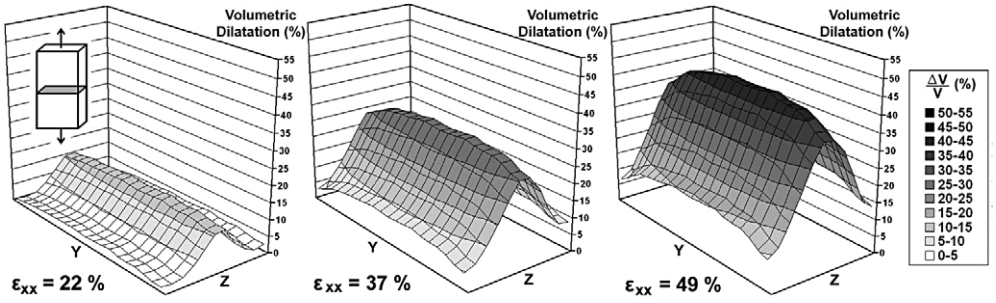

Fig. 10. Evolution of experimental volumetric dilatation extrapolated by projection in the specimen cross-section for composite B.

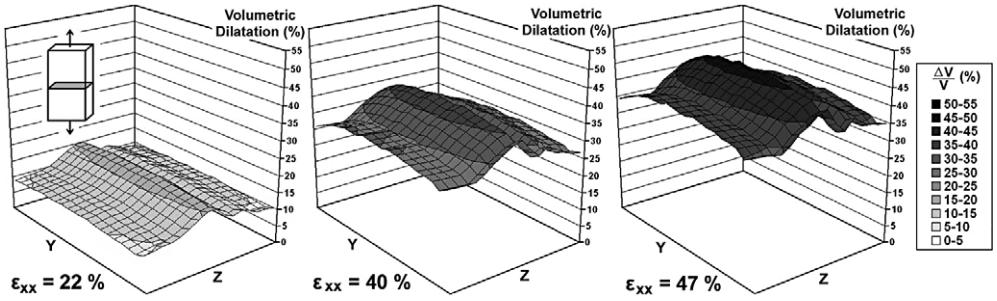

Fig. 11. Evolution of experimental volumetric dilatation extrapolated by projection in the specimen cross-section for composite A.

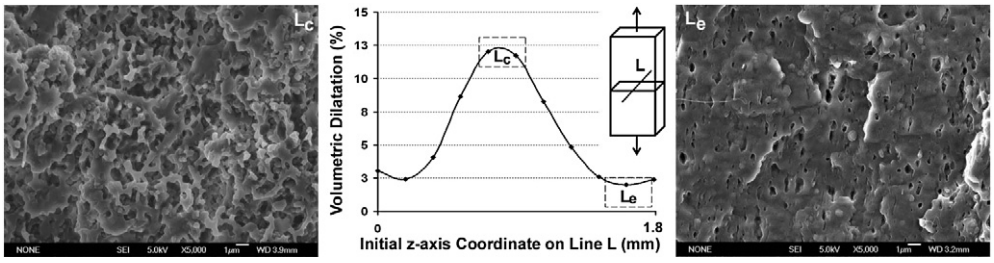

Fig. 12. Comparison of measured volumetric dilatation values and microstructure observations by SEM in deformed impact-modified polypropylene B for $\varepsilon_{xx} = 22\%$: L_c, in the specimen core; L_e, at the edges.

cross-section of the composite B specimen. It corresponds to a section of volumetric dilatation maps presented in Fig. 10 for an average axial strain ε_{xx} of 22%. One can see again the high volumetric dilatation gradient in this material. These measurements have been compared with the corresponding material microstructure.

The deformed microstructure of composite B has been observed by SEM after the specimen was deformed up to 22% of axial strain. The specimen was broken by cryogenic fracture and the observations were performed in the cross-section. Fig. 12 presents the deformed microstructure of composite B. One observation has been made in the specimen core (L_c) and the other has been performed close to the surface (L_e).

On these micrographs, small black areas correspond to the presence of voids. The microstructure observed in the specimen core (L_c) shows numerous voids, leading to a quasi "spongy" material. On the other hand, the micrograph recorded close to the surface (L_e) shows a smaller quantity of voids.

Comparison of these microstructural observations demonstrates that damage process is highly advanced in specimen core, whereas near the surface, few cavitations can be observed. These observations are in agreement with the volumetric dilatation gradients experimentally determined with the 3D DIC technique: in this composite, during tension test, the void formation is much higher in the specimen core than in the edges.

6. Conclusion

A 3D DIC technique has been developed in order to get numerical images of both front and lateral sides of the specimen with a unique camera and with a small scale factor. The fine grainy pattern applied on both surfaces allowed us to measure in-plane displacement in the three directions with a spatial resolution of about $0.45 \times 0.45\ \text{mm}^2$. Thereby, it is possible to determine accurately the full-field strains in three directions all along tension tests.

Applied to impact-modified polypropylenes, this technique shows the development of high anisotropic transverse strains in the composite. The analysis of in-plane strain fields also put in light that impact-modified polypropylenes deform with large transverse strain gradients.

Those gradient considerations introduce a new way of investigation of polymers volumetric behaviour. Assuming that specimen faces are representative of "inside" deformation, the local strains measured on front and lateral faces of specimens have been projected, respectively, on z- and y-axis. Thus, volumetric dilatation maps can be plotted in specimen cross-section.

Analysing volumetric dilatation maps in specimen cross-section, two volumetric behaviours have been identified for the studied composites A and B. When the talc content is only 1%, there is a very large gradient of the volumetric dilatation which is almost three times higher in the specimen core than in the edges. But, this phenomenon is significantly reduced in composite A filled with 4% of talc.

This is in agreement with microscopic observations. These results highlight the influence of talc presence on deformation mechanisms in impact-modified polypropylenes.

The development of sensitive 3D DIC technique is a new step in material behaviour study, allowing to measure anisotropic, volumetric and heterogeneous strains.

Acknowledgements

We would like to thank the ADEME (Agence pour le Développement de l'Environnement et de la Maîtrise des Energies), the Région Poitou-Charentes and Research Ministry – through ACI Recypro B – for sponsoring this work.

References

[1] G'Sell C, Marquez-Lucero A. Determination of the intrinsic stress/strain equation of thin polymer films from stretching experiments under plane-strain tension. Polymer 1993;34(13):2740–9.
[2] Nazarenko S, Bensason S, Hiltner A, Baer E. Effect of temperature and pressure on necking of polycarbonate. Polymer 1994;35(18):3883–91.
[3] Haynes AR, Coates PD. Semi-automated image analysis of the true tensile drawing behaviour of polymers to large strains. J Mater Sci 1996;31(7):1843–55.
[4] Parsons E, Boyce MC, Parks DM. An experimental investigation of the large-strain tensile behavior of neat and rubber-toughened polycarbonate. Polymer 2004;45(8):2665–84.
[5] Buisson G, Ravi-Chandar K. On the constitutive behaviour of polycarbonate under large deformation. Polymer 1989;31(11):2071–6.

[6] Lagattu F, Brillaud J, Lafarie-Frenot MC. High strain gradient measurements by using digital image correlation technique. Mater Charact 2004;53(1):17–28.
[7] Laraba-Abbesa F, Ienny P, Piques R. A new 'tailor-made' methodology for the mechanical behaviour analysis of rubber-like materials: I. Kinematics measurements using a digital speckle extensometry. Polymer 2002;44(3):807–20.
[8] G'Sell C, Hiver JM, Dahoun A. Experimental characterization of deformation damage in solid polymers under tension, and its interrelation with necking. Int J Solid Struct 2002;39(13–14): 3857–72.
[9] Gloaguen JM, Lefebvre JM. Plastic deformation behaviour of thermoplastic/clay nanocomposites. Polymer 2001;42(13):5841–7.
[10] Pukanszky B, Belina K, Rockenbauer A, Maurer FHJ. Effect of nucleation, filler anisotropy and orientation on the properties of PP composites. Composites 2004;25(3):205–14.
[11] Zebarjad SM, Sajjadi SA, Tahani M. Influence of filler particles on deformation and fracture mechanism of isotactic polypropylene. J Mater Process Technol 2005;155–156:1459–64.
[12] Grein C, Plummer CJG, Kausch HH, Germain Y, Béguelin P. Influence of β nucleation on the mechanical properties of isotactic polypropylene and rubber modified isotactic polypropylene. Polymer 2002;43(11):3279–93.
[13] Parsons E, Boyce MC, Parks DM, Weinberg M. Three-dimensional large-strain tensile deformation of neat and calcium carbonate-filled high-density polyethylene. Polymer 2005;46(7):2257–65.
[14] Brillaud J, Lagattu F. Limits and possibilities of laser speckle and white light image correlation methods: theory and experiments. Appl Opt 2002;41:6603–13.
[15] Pannier Y, Avril S, Rotinat R, Pierron F. Identification of elasto-plastic constitutive parameters from statically undetermined tests using the virtual fields method. Exp Mech 2006;46:735–55.